GEOPHYSICS, VOL. 67, NO. 2 (MARCH-APRIL 2002); P. 604–609, 6 FIGS.
10.1190/1.1468621

# 3-D imaging using higher order fast marching traveltimes

Alexander Mihai Popovici* and James A Sethian‡

**ABSTRACT**

Recently, fast marching methods (FMM) beyond first order have been developed for producing rapid solutions to the eikonal equation. In this paper, we present imaging results for 3-D prestack Kirchhoff migration using traveltimes computed using the first-order and second-order FMM on several 3-D prestack synthetic and real data sets. The second order traveltimes produce a much better image of the structure. Moreover, insufficiently sampled first order traveltimes can introduce consistent errors in the common reflection point gathers that affect velocity analysis. First-order traveltimes tend to be smaller than analytic traveltimes, which in turn affects the migration velocity analysis, falsely indicating that the interval velocity was too low.

## INTRODUCTION

Kirchhoff migration is recognized as a comprehensive and flexible method of imaging prestack 3-D seismic data because of its ability to image complex geological structures and handle irregularly sampled data. Kirchhoff migration images seismic data by approximately solving the wave equation with a boundary integral method and using an imaging condition. The acoustic reflectivity at every point of the earth's interior is computed by summing the recorded data over multidimensional surfaces; the shape of the summation surfaces and the summation weights are computed from the Green's functions of the single-scattering wave-propagation experiment. Green's functions are usually approximated by solving the eikonal equation which is a high frequency approximation to the acoustic wave equation.

Fast marching methods (FMM), introduced by Sethian (1996), are fast techniques for solving the eikonal equation. They have been recently used to generate Green's function tables through the use of a fast 3-D traveltime computation (Popovici and Sethian, 1997; Sethian and Popovici, 1999). FMM compute the viscosity solution to the eikonal equation in $O(N \log N)$ time, where $N$ is the total number of points in the computational domain. The techniques are based on a marriage of upwind finite difference operators for entropy-satisfying gradients, the theory of viscosity solutions to Hamilton-Jacobi equations, and fast sorting algorithms. The methods are unconditionally stable, can be used in any orthogonal coordinate system, and globally construct the solution to the eikonal equation for each point in the coordinate domain in the presence of arbitrarily large discontinuities in the velocity model. In addition, the method resolves any overturning propagation wavefronts.

FMM belong to a class of methods known as Dijkstra-like, in that they are closely connected to Dijkstra's fundamental technique for finding shortest paths on weighted graphs (Dijkstra, 1959). Dijkstra's method is not consistent with the eikonal equation in that as the number of network path links increases, the solution does not converge to the underlying partial differential equation for traveltimes. FMM replace the operator in Dijkstra's method with viscosity-satisfying upwind finite-difference schemes in such a way that the resulting method is stable, consistent, and converges to the correct viscosity eikonal solution while maintaining the underlying speed of the Dijkstra's network path algorithm.

The original version of the FMM was designed using a first-order approximant to the gradient in the eikonal equation $|\nabla T| = F(x, y, z)$. These upwind first-order approximations select the viscosity solution by choosing the correct direction of the upwinding. This yields a highly efficient algorithm; however, the use of first-order operators means that the computed solution along diagonals lags behind those along grid lines. For example, in computing the solution to the simple eikonal $|\nabla T| = 1$, which yields the distance from a source to any point $(x, y, z)$, the computed solution has no error along any grid line that intersects the source, and varies most profoundly along the diagonal. The error term is largest along the diagonal because in the Taylor expansion for the solution, the cross term is least accurate along the diagonal and acts as an extra smoothing term. The results of this are evident when using a grid over a large physical domain, in which the traveltimes errors are substantial, as shown in Figure 1. Because of this, several authors

Manuscript received by the Editor February 7, 2000; revised manuscript received July 19, 2001.
*3DGeo Development, 465 Fairchild Drive, Suite 226, Mountain View, California 94043. E-mail: mihai@3dgeo.com.
‡University of California, Department of Mathematics, Berkeley, California 94720. E-mail: sethian@math.berkeley.edu.
© 2002 Society of Exploration Geophysicists. All rights reserved.

have adapted the method to spherical, cylindrical, or tetragonal meshes in order to better align with the expanding wave front from a point source (Alkhalifah and Fomel, 1997; Sun and Fomel, 1998). In the case of a uniform slowness velocity, this has some advantages. However, for a nonuniform slowness velocity, the lead wave can bend and contort and, in fact, in some places move in a direction unaligned with this grid, substantially increasing the error.

Recently, Sethian (1999) introduced higher order FMM by employing higher order approximants to the gradient through the use of a switch function. This higher order Cartesian scheme is a small modification of the original algorithm and satisfies both requirements for accuracy and computational efficiency. The basic idea relies on a decomposition of the higher order stencil into higher order terms and a first-order term. Using a switch function, the higher order terms are zeroed in the presence of discontinuity lines in the eikonal field; in such areas where the gradient of the field is discontinuous, the method falls back on the first-order scheme. In smooth regimes, higher order stencils are used. This scheme adds negligible cost to the overall computation while considerably improving the accuracy, as demonstrated by Rickett and Fomel (1999).

In this paper, we consider the application of these higher order schemes to computation of traveltimes. The second-order traveltimes produce higher resolution images when used for 3-D and 2-D prestack Kirchhoff depth migration. In two dimensions, the imaging error is not as significant as in three dimensions, as explained in the imaging results section below. We use the 2-D Marmousi, the 3-D SEG/EAGE salt model, and a 3-D North Sea data set to show imaging improvements when using a second-order stencil. We find that the accuracy improvement is especially important for migration velocity analysis, where first-order errors affect the common reflection point (CRP) gathers. The events in the CRP gathers appear to curve up, falsely indicating the migration velocity is too slow. We conclude that second-order methods should be used for most 3-D prestack imaging methods.

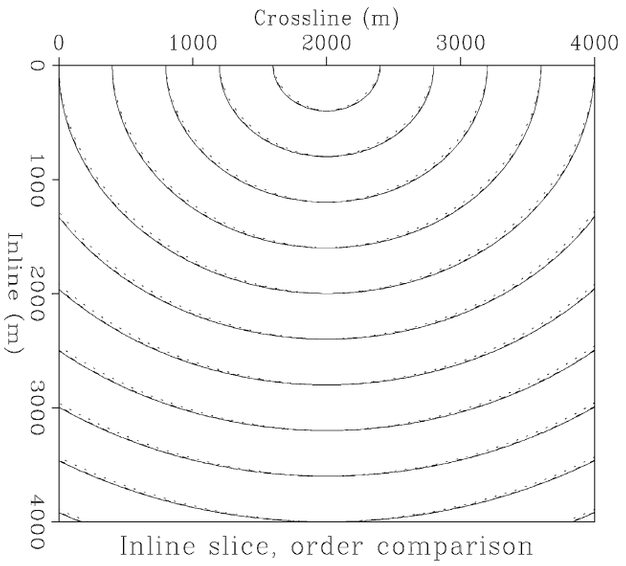


FIG. 1. Analytic, first-order, and second-order computations on a $200 \times 200 \times 200$ grid. In-line section through the middle of the cube. Solid = exact solution; short dashes = first order; long dashes = second order.

## HIGHER ORDER FAST MARCHING METHODS

The FMM solves the eikonal equation by systematically constructing the traveltimes in an upwind fashion. The algorithm is made fast by confining the "building zone" to a narrow band around the front. The idea is to sweep the front ahead in an upwind fashion by considering a set of points in a narrow band around the existing front and to march this narrow band forward, freezing the values of existing points and bringing new ones into the narrow band structure.

The FMM was originally implemented as a first-order scheme, using first-order operators in the finite difference approximations. While fine grids are possible because of the tremendous speed of these techniques (traveltimes on a $100 \times 100 \times 100$ grid in a complex velocity model can be obtained in 10 s on a 200-MHz Origin 2000 node), some grid effects are seen due to numerical diffusion which is most pronounced along grid diagonals. Thus, arrival times along diagonals are not as accurate as those along grid lines, and this is manifested in a grid error. Figure 1 shows the errors are maximum in the diagonal direction, and minimum along the grid axes.

Attempts to focus on building a higher order method by replacing the operators with higher order approximants often become complex due to the delicacy of the causality relationship (Kim and Cook, 1999). In other words, the systematic advancement of the solution field relies on the fundamental upwinding. Any attempt to go back and "fix" values means that one has destroyed this view and runs the risk of creating a technique of the same complexity as pure iteration.

Recently the basic FMM was extended to second order (Sethian, 1999). In brief, the operator becomes second order or higher when there are enough accepted values behind the stencil. By using a switch function, one can build a one-sided second-order stencil whenever upwind and previously accepted points are available. In all other cases, the operator reverts to first order. The ultimate accuracy of this scheme depends on the distribution of points where the scheme reverts to first order; loosely speaking, if points where the switch reverts to first order are limited to those only directly connected to shock lines in the eikonal solution, then the method approaches second order.

The higher order switch function has been designed in the context of FMM, and is meant to couple with the considerable computational efficiency inherent in those approaches that result from the combination of causality and sorting. However, we note that the fundamental idea may also be used in other eikonal solvers, including essentially nonoscillatory-based approaches (Kim and Cook, 1999) and wavefront approaches (Qin et al., 1992).

Higher order FMM may be built as follows. Begin by noting that a second-order backward approximation to the first derivative $T_x$ in the eikonal equation is given by

$$T_x \approx \frac{3T_i - 4T_{i-1} + T_{i-2}}{2\Delta x},$$

which may be compactly written as

$$T_x \approx D^{-x}T + \frac{\Delta x}{2} D^{-x-x}T,$$

where we used the standard finite-difference notation that

$$D^{-x}T = \frac{T_i - T_{i-1}}{h} \quad D^{-x-x}T = \frac{T_i - 2T_{i-1} + T_{i-2}}{h^2},$$

where $T_i$ is the value of $T$ on a grid at the point $ih$ with grid spacing $h$. A similar expression holds for the forward difference, namely,

$$T_x \approx D^{+x}T - \frac{\Delta x}{2} D^{+x+x}T.$$

Consider now the switch functions defined by (the expressions are similar in $y$ and $z$)

$$\text{switch}_{\text{ijk}}^{-\text{x}} = \begin{bmatrix} 1 & \text{if } T_{i-2,j,k} \text{ and } T_{i-1,j,k} \text{ are known} \\ 0 & \text{if not} \end{bmatrix},$$

$$\text{switch}_{\text{ijk}}^{+\text{x}} = \begin{bmatrix} 1 & \text{if } T_{i+2,j,k} \text{ and } T_{i+1,j,k} \text{ are known} \\ 0 & \text{if not} \end{bmatrix}.$$

One can then use these operators in the FMM by inserting them in the standard upwind stencil, as follows:

$$\begin{bmatrix} \max\left[\left[D_{ijk}^{-x}T + \text{switch}_{ijk}^{-x}\frac{\Delta x}{2}D_{ijk}^{-x-x}T\right], -\left[D_{ijk}^{+x}T - \text{switch}_{ijk}^{+x}\frac{\Delta x}{2}D_{ijk}^{+x+x}T\right], 0\right]^2 \\ + \\ \max\left[\left[D_{ijk}^{-y}T + \text{switch}_{ijk}^{-y}\frac{\Delta y}{2}D_{ijk}^{-y-y}T\right], -\left[D_{ijk}^{+y}T - \text{switch}_{ijk}^{+y}\frac{\Delta y}{2}D_{ijk}^{+y+y}T\right], 0\right]^2 \\ + \\ \max\left[\left[D_{ijk}^{-z}T + \text{switch}_{ijk}^{-z}\frac{\Delta z}{2}D_{ijk}^{-z-z}T\right], -\left[D_{ijk}^{+z}T - \text{switch}_{ijk}^{+z}\frac{\Delta z}{2}D_{ijk}^{+z+z}T\right], 0\right]^2 \end{bmatrix}^{1/2} = F_{ijk}, \quad (1)$$

where $F_{ijk}$ is the slowness field.

This scheme attempts to use a second-order one-sided upwind stencil whenever points are available, but reverts to a first-order scheme in the other cases. In most cases, as the number of grid points is increased for a given velocity model, second-order convergence is obtained in both the $L_2$ and $L_\infty$ norm. Third and higher order versions of FMM can be implemented in a straightforward similar manner; the degree to which these higher order local approximations produce equivalent global higher order schemes depends on the underlying complexity of the field (Sethian, 1999).

In Figures 1 and 2, we display the exact solution, the first-order scheme, and the second-order scheme to compute traveltimes in a constant velocity model. For the vertical in-line slice through the traveltime cube shown in Figure 1, the second-order solution is almost superimposed on the analytical solution. The largest error between the first order and the analytical solution appears on the diagonal. This is consistent with the error discussion in Sethian and Popovici (1999). In the depth slice shown in Figure 2, the difference between the three solutions is more visible, and the second order-method provides a considerably more accurate solution.

## IMAGING EXAMPLES

Two-dimensional FMM traveltimes were used to image the Marmousi data, a well-known prestack synthetic data set generated by the Institut Français du Pétrole. The Marmousi data set is based on a real geologic model from the Cuanza Basin in Angola (Bourgeois et al., 1991). Figure 3 compares the prestack depth migration images obtained using first-order and second-order traveltimes. The continuity of the events on the right side of the faults is better in the second-order image, and also the image of the right fault has better definition. As shown in Figure 1, in two dimensions the first-order solution differs from the second-order solution mainly along the diagonal directions. The Kirchhoff summation operator in two dimensions is a curve, and the percentage of points along the curve where the two solutions differ is much smaller in two dimensions than in three dimensions. In the 3-D case, the Kirchhoff summation is performed along surfaces, and there are more points where the first-order solution differs from the second-order solution, as can be seen in Figure 2.

Next, we compare the 3-D FMM first-order and second-order traveltime algorithms by imaging the 3-D SEG/EAGE salt dome A1 data set (Aminzadeh et al., 1996). The SEG/EAGE salt dome model was designed to contain major complex features that are typical of complex Gulf of Mexico salt

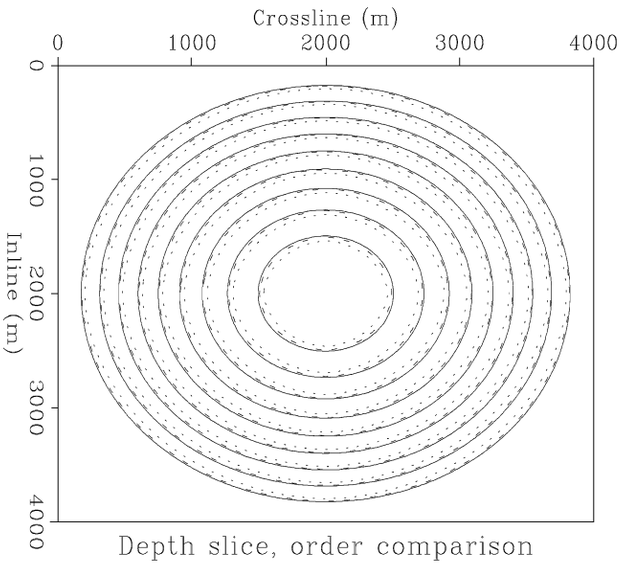


FIG. 2. Analytic, first-order, and second-order computations on a $200 \times 200 \times 200$ grid. Depth slice through the traveltime cube. Solid = exact solution; short dashes = first order; long dashes = second order.

structures. It includes a northwesterly plunging stock, a secondary reactivation crest southward of the stock, a low-relief eastern flank, a faulted southern flank with a toe thrust, a rounded overhang on the west flank, five sands that are gas charged (at least one contains both a gas/oil and an oil/water contact), and a shale sheath that is modeled to be geopressured. The sea floor map exhibits a counter-regional fault scarp, a bathymetric rise associated with the sill crest, and a shelf break at the southeast end of the model.

The classic A1 data set simulates a 138-shot marine acquisition survey using six streamers with 65 groups per streamer. The group interval is 40 m, streamer spacing is 80 m, near offset is 160 m, and far offset is 2760 m. Thus, the geometry is 3-D swath. Figure 4 shows a comparison of migrated lines from the

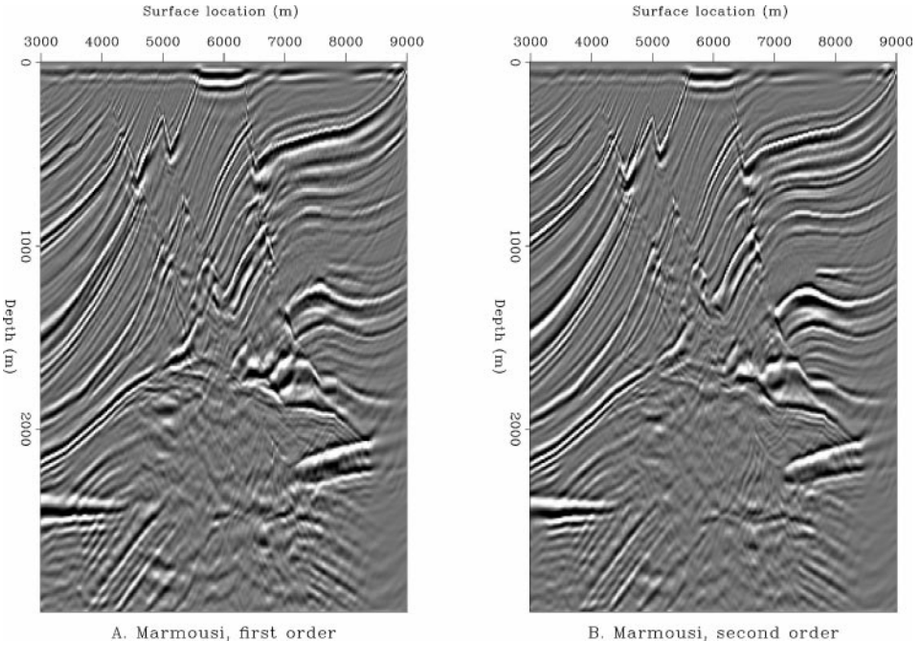


FIG. 3. Two-dimensional migration of the Marmousi data set. (a) First-order FMM traveltimes. (b) Second-order FMM traveltimes. In two dimensions, the difference between first-order and second-order imaging results is small.

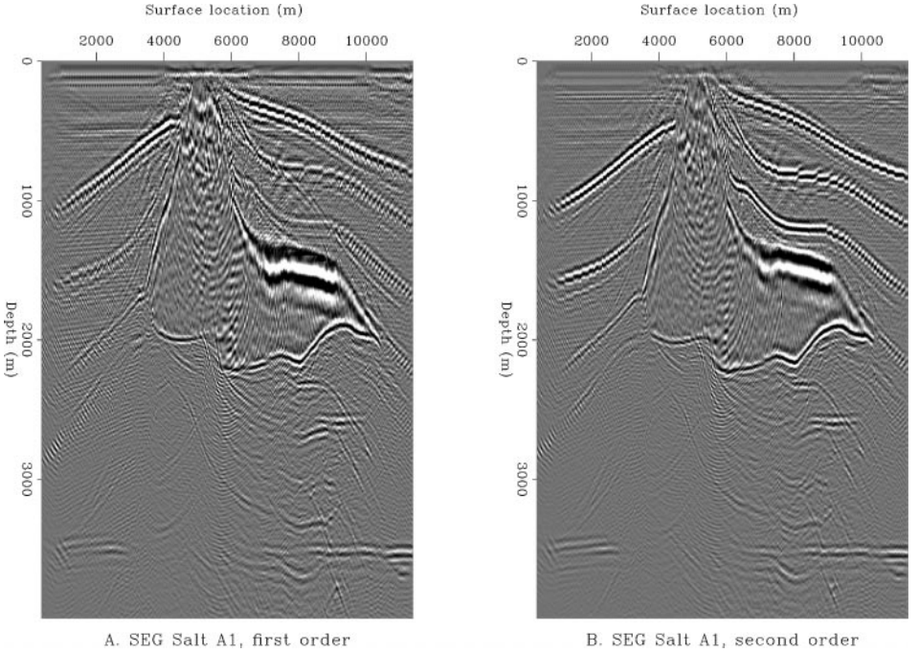


FIG. 4. Three-dimensional migration line through the SEG/EAGE salt model. (a) In-line slice using first-order FMM traveltimes. (b) In-line slice using second-order FMM traveltimes. In three dimensions, the difference between first-order and second-order imaging is greater than in two dimensions because the traveltime solution deviates from the analytic solution in a larger percentage than in two dimensions.

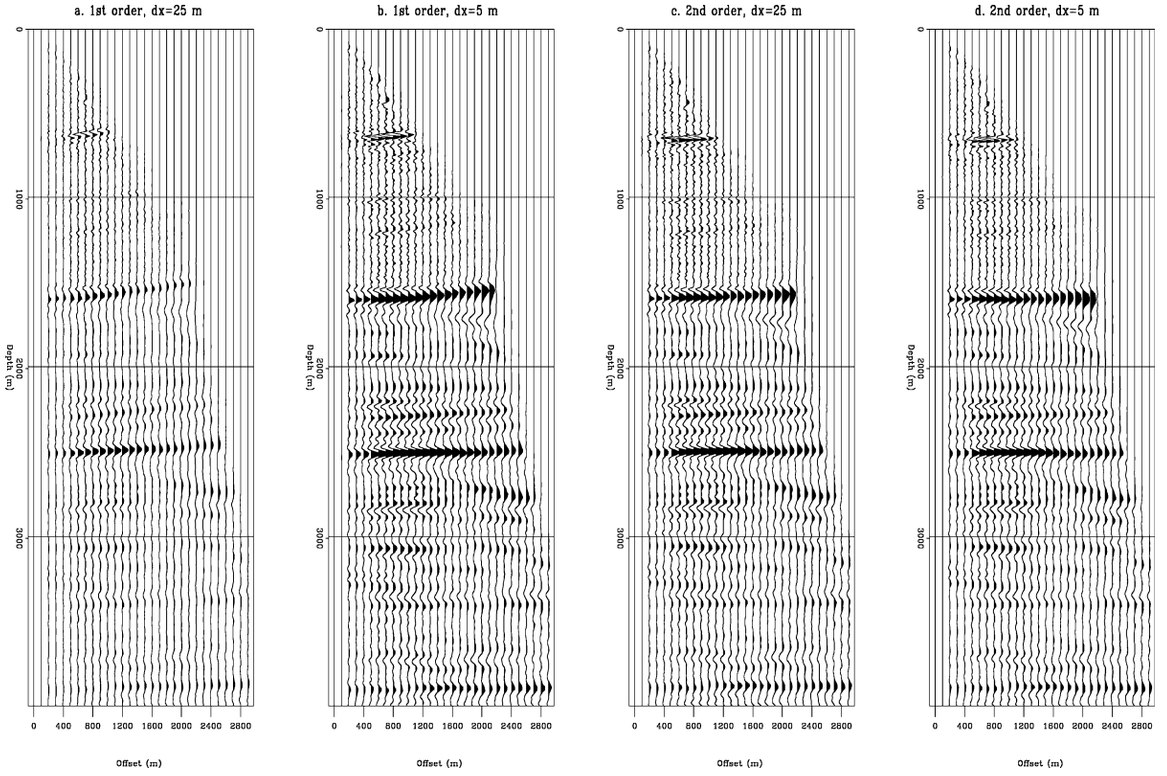


FIG. 5. Comparison of CRPs migrated using first-order and second-order traveltimes with different grid sampling. (a) First-order traveltimes, 25-m grid sampling. (b) First-order traveltimes, 5-m grid sampling. (c) Second-order traveltimes, 25-m grid sampling. (d) Second-order traveltimes, 5-m grid sampling. Such differences will falsely affect the migration velocity analysis.

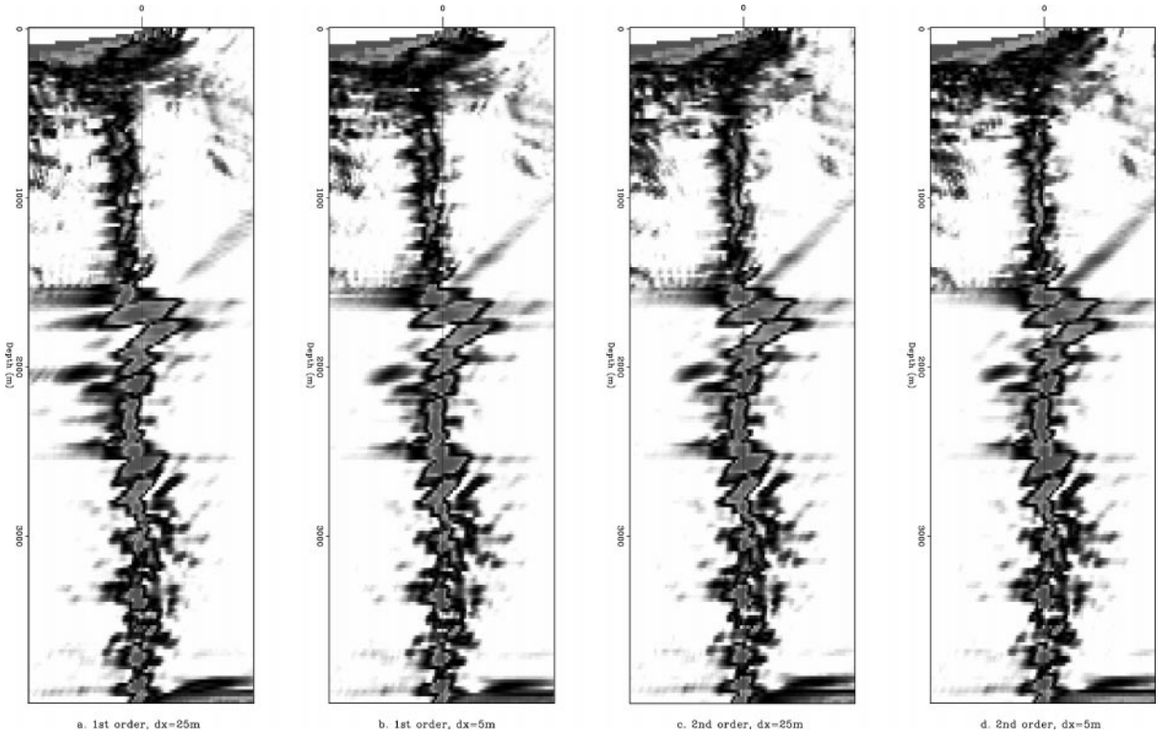


FIG. 6. Comparison of residual slowness semblance scans. (a) First-order traveltimes, 25-m grid sampling. (b) First-order traveltimes, 5-m grid sampling. (c) Second-order traveltimes, 25-m grid sampling. (d) Second-order traveltimes, 5-m grid sampling.

data set. Notice the improved resolution in Figure 4b of the sediment reflections, especially the second and third one on the right side of the salt dome, and the overall reduction in migration artifacts. The absence of artifacts is also especially notable under salt. In three dimensions, the effect of higher accuracy using second-order traveltimes is more apparent than in two dimensions.

Figure 5 shows a comparison of migrated CRP gathers in a real North Sea 3-D data set, using different grid sampling for building the 3-D traveltime tables. The traveltime tables have a grid sampling of 25 m and 5 m. The first two CRPs were imaged using first-order traveltimes, whereas the last two CRPs used second-order traveltimes. Examining the strong event at 1600 ms, we observe that in the first-order case, even after reducing the grid size to 5 m, the event curves up, indicating the background migration velocity was too low. The event appears flat in the second order CRPs. For the first order, even after reducing the grid sampling to 5 m, which is impractical for realistic situations, the error will affect the velocity analysis performed on the CRPs. The event at 1600 m still presents some residual moveout that would require to increase the migration velocity. In the second-order case, the improvement in reducing the grid size are insignificant, and judging from the flatness of the deeper events, the velocity model seems adequate.

Corresponding to the four CRP gathers, in Figure 6 we show the residual slowness semblance scans that are input to the migration velocity analysis update. The convention in these residual slowness scans is that events that are migrated with too slow velocity appear as negative values, whereas events migrated with too high velocity appear as positive values. Events migrated with the correct velocity are lined up on the zero line. In Figure 6, we observe that first-order traveltimes bias the scan toward negative values, implying that the migration velocity is too small. Higher order traveltimes show that, in fact, the velocity difference is much smaller. In the second-order panels, the differences between the 5-m grid and 25-m grid are insignificant. Also, the semblance scans in the second-order panels have a tighter definition of the semblance events down to 1500 m, evidence of better event focusing. We conclude that using first-order traveltimes can introduce an additional error in the migration velocity analysis loop.

## CONCLUSIONS

We analyze the effect of second-order fast eikonal solvers in the calculation of traveltimes. We show 3-D prestack Kirchhoff migration comparisons using first-order and second-order traveltimes, and conclude that the image is improved considerably using second-order traveltimes. Moreover, we show that the error introduced by first order-methods can not be sufficiently handled by reducing the traveltime grid size and that such errors can affect migration velocity analysis.

## REFERENCES


Alkhalifah, T., and Fomel, S., 1997, Implementing the fast marching eikonal solver: Spherical versus Cartesian coordinates: Stanford Exploration Project Report, **95**, 149–171.

Aminzadeh, F., Burkhard, N., Long, J., Kunz, T., and Duclos, P., 1996, Three dimensional SEG/EAEG models—An update: The Leading Edge, **15**, 131–136.

Bourgeois A., Bourget M., Lailly P., Poulet M., Ricarte P., and Versteeg R., 1991, Marmousi, model and data: Proceedings of the 1990 EAEG workshop on Practical Aspects of Seismic Data Inversion.

Dijkstra, E. W., 1959, A note on two problems in connection with graphs: Numerische Mathematik, **1**, 269–271.

Kim, S., and Cook, R., 1999, 3-D traveltime computation using second-order ENO scheme: Geophysics, **64**, 1867–1876.

Popovici, A. M., and Bevc, D., 1997, 3-D prestack depth migration of the SEG/EAGE salt model: 67th Ann. Internat. Mtg., Soc. Expl. Geophys., Expanded Abstracts, 1086–1089.

Popovici, A. M., and Sethian, J. A., 1997, Three-dimensional traveltime computation using the fast marching method: 67th Ann. Internat. Mtg., Soc. Expl. Geophys., Expanded Abstracts, 1778–1781.

Qin, F., Luo, Y., Olsen, K. B., Cai, W., and Schuster, G. T., 1992, Finite difference solution of the eikonal equation along expanding wavefronts: Geophysics, **57**, 478–487.

Rickett, J., and Fomel, S., 1999, A second-order fast marching eikonal solver: Stanford Exploration Project Report, **100**, 287–293.

Sethian, J. A., 1996, Level set methods: Cambridge Univ. Press.

——— 1999, Level set methods and fast marching methods: Evolving interfaces in computational geometry, fluid mechanics, computer vision and materials science: Cambridge Univ. Press.

Sethian, J. A., and Popovici, A. M., 1999, Three dimensional traveltime computation using the fast marching method: Geophysics, **64**, 516–523.

Sun, Y., and Fomel, S., 1998, Fast marching eikonal solver in the tetragonal coordinates: Stanford Exploration Project Report, **97**, 241–250.